

June 30, 2003

Martha Symko-Davies
Senior Project Leader, MS 3214
Subcontract Technical Monitor
National Renewable Energy Laboratory
1617 Cole Boulevard
Golden, CO 80401-3393

RE: quarterly report-Univ. of Toledo-Phase 2, Quarter 3

Dear Martha,

This is the progress report for the Eighth Quarter of Subcontract No. AAT-1-30620-09, "Polycrystalline Thin-Film Tandem Photovoltaic Cells," for the period March 1, 2003 – May 31, 2003. This subcontract employs magnetron sputter deposition and vapor transport deposition of II-VI semiconductors for exploratory development of four-terminal and two-terminal tandem solar cells based on CdTe alloys for top cells. The effort, at the U. of Toledo and First Solar, LLC, includes exploratory work on a transparent back contact as well as a suitable tunnel junction to a bottom cell. The Institute of Energy Conversion is providing support for various characterization and tandem cell design issues. Reports from First Solar and from IEC are included as Sections C and D, respectively.

During this quarter, we presented several papers on our HiPerfPV work, three at the Materials Research Society spring symposium and two papers at the 3rd World Conference on PV in Osaka. The three MRS papers are: 1) A. Gupta and A.D. Compaan, "14% CdS/CdTe Thin Film Cells with ZnO:Al TCO," oral paper B3.9; 2) A. Gupta, K. Allada, S-H. Lee, and A.D. Compaan, "Oxygenated CdS Window Layer for Sputtered CdS/CdTe Solar Cells," poster paper B8.9, and 3) J. Drayton, V. Parikh, G. Rich, A. Gupta, T. Osborn, R.G. Bohn, and A.D. Compaan, "Sputtered ZnTe:N and ZnO:Al for Solar Cell Electrodes and Recombination Junctions," poster paper B8.11. The two Osaka papers are: 4) A. Gupta and A.D. Compaan, "All sputtered 14% CdS/CdTe device with ZnO:Al front contact," oral paper 2O-C10-02 (selected as one of the highlights in the conference summary), and 5) A.D. Compaan, J. Drayton, V.Y. Parikh, G. Rich, A. Gupta, C. Taylor, Y. Yu, T. Osborn, and R.G. Bohn, "ZnTe:N/ZnO:Al recombination junctions and stability properties of ZnTe:N and ZnO:Al," poster 2P-A8-31. A preprint of submitted paper #2 was attached to the previous quarterly report. Preprints of papers #4 and #5 are attached/appended to this report.

Yours truly,

Alvin D. Compaan, P.I.

Copies to: Carolyn Lopez, Subcontract Associate, MS 2713, NREL (hard copy)
Upali Jayamaha, Lower-tier subcontractor P.I. (electronic)
Brian McCandless, Lower-tier subcontractor P.I. (electronic)
V. Karpov, X. Deng, co-Investigators (electronic)
Dorothy Spurlock, Director, Research and Sponsored Programs (hard copy)

Attachments: 1) manuscript for WCPEC-3: A. Gupta and A.D. Compaan, "All sputtered 14% CdS/CdTe device with ZnO:Al front contact"
2) manuscript for WCPEC-3: A.D. Compaan, J. Drayton, V.Y. Parikh, G. Rich, A. Gupta, C. Taylor, Y. Yu, T. Osborn, and R.G. Bohn, "ZnTe:N/ZnO:Al recombination junctions and stability properties of ZnTe:N and ZnO:Al"

A. CdZnTe, CdMnTe, and HgCdTe alloy films and cells--update

Work continues on postdeposition treatments of the alloys CdZnTe and CdMnTe. Most of the effort in this quarter has focused on the use of H_2+Ar ambients during the $CdCl_2$ processing. This is motivated by the observation that $CdCl_2$ processing in the presence of oxygen leads to the formation of ZnO (See the IEC report in a later section.) and reduction of Zn/Cd ratios in the films. Details will be reported in our next report, but we find that if a pre-anneal is performed in H_2+Ar without $CdCl_2$ at about $520^\circ C$, the cell performance above 7% can be obtained for

sputtered cells ($V_{OC}=737$ mV, $J_{sc}=19$ mA/cm², FF =51%).

However, the QE indicated an absorption edge only slightly blue-shifted from that of pure CdTe and the SEM/EDS indicates $x=0.05$ even though the as-deposited films had $x=0.35$. Roughly similar behavior occurs for VTD CdZnTe devices and for sputtered CdMnTe alloy devices after $CdCl_2$ processing.

Work also continues on HgCdTe alloy devices with efforts to introduce extrinsic doping through reactive sputtering with $N_2 + Ar$ as the sputter gas. 13 of the 22 films and devices made during this period used 5% N_2 in Ar. We find that the use of N_2 in the sputter gas does not shift the (~ 1.0 eV) band gap of the as-deposited device. However, the resistivity of the as-deposited films is little affected by the reactive sputtering, although postdeposition annealing at 390 C in air or in N_2 does indicate a drop in resistivity by a factor of 10 to 100 in the reactively sputtered films. After chloride treatment, the bandgap remains near 1 eV, but best device performance has not exceeded 2.5%.

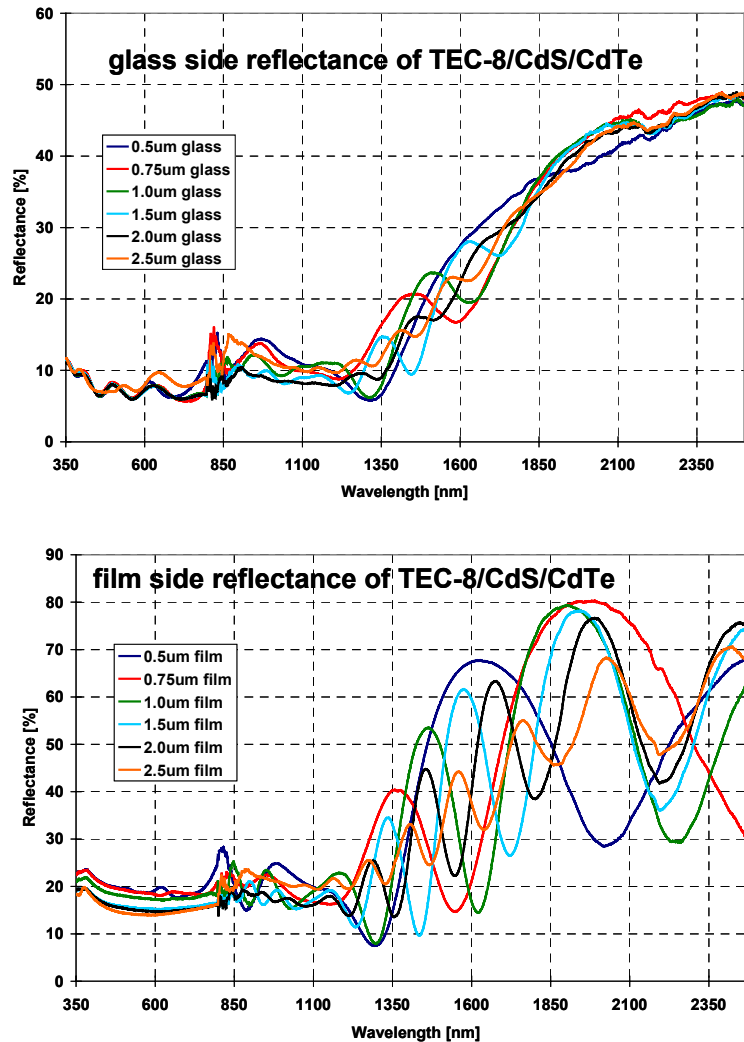


Fig. 1 Integrating sphere reflection from TEC-8 /CdS/CdTe structures for various CdTe thicknesses.

B. T & R of CdS/CdTe cell structures vs. CdTe thickness

In this report we shall provide more detailed information on transmission and reflectivity studies of cell structures glass/SnO₂:F/CdS(0.13 μ m)/CdTe as a function of CdTe thickness.

The reflectivity data were obtained with the integrating sphere for incidence either from the glass side or the film side. The reflection data, shown in Fig. 1, clearly show higher reflectivity in the 350-850 nm region from the film side due to the large index of refraction discontinuity at the air/CdTe interface. This is suppressed from the glass side. Relatively small changes are observed due to the CdTe thickness for wavelengths below \sim 1200 nm.

Transmission data were obtained in both line-of-sight and integrating sphere modes so that the interference and scattering effects could be observed. The transmission data, shown in Fig. 2, exhibits the partial transmission below 800 nm of the thinner CdTe structures. In the 850-1200 nm region important for the bottom cell, the effects of scattering noticeably reduce the transmission only for the two thicker CdTe structures (2.0 μ m and 2.5 μ m). Preliminary comparisons between sputtered and VTD-deposited structures in the range of 2.5 to 3.0 μ m indicate noticeably more scattering for the high temperature, larger-grain-size VTD material. This will be a critically important consideration especially for four-terminal tandem devices, but grain boundary scattering, *etc.*, is likely also to impact two-terminal tandem devices.

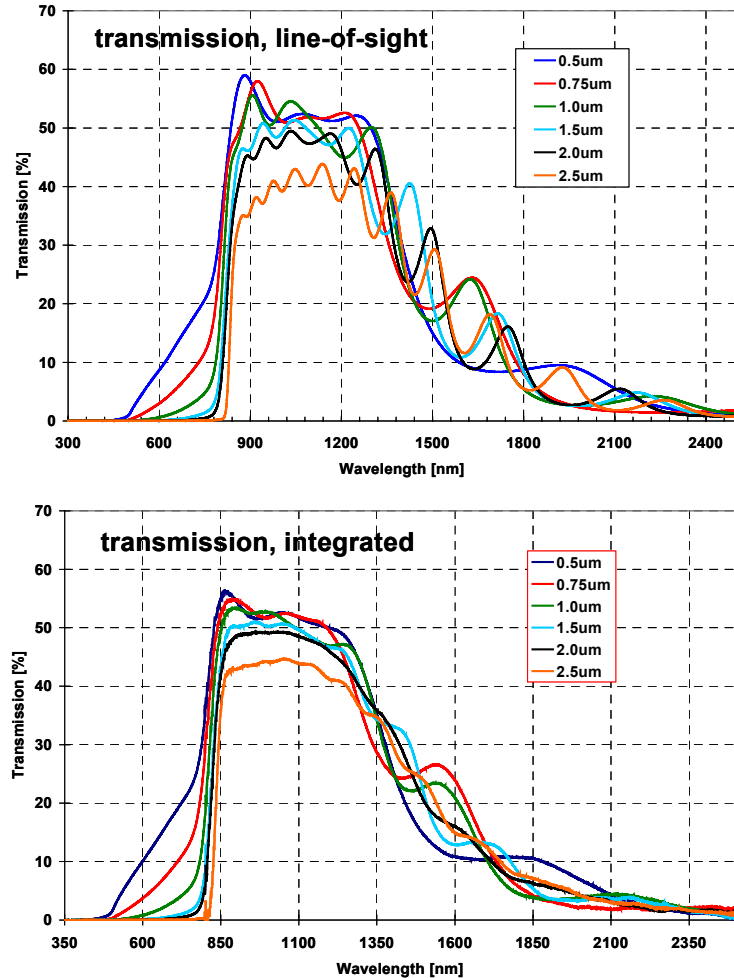


Fig. 2 Line-of-sight and integrating sphere transmission through TEC-8/CdS/CdTe structures for several CdTe thicknesses.

C. First Solar activities: sputtering and postdeposition treatments of CTO and CdS

Key Results

- A more consistent/robust method of annealing cadmium stannate films perfected.
- Cadmium stannate films grown at rates as high as 500 Å/minute showed good electro optical properties after annealing
- Near 14% efficient cells fabricated on CTO based superstrates
- Cadmium sulfide and zinc stannate targets ordered for the large sputter coater

Cadmium Stannate (CTO)

-Previously we have been annealing as-grown CTO films by placing them face down on a CdS source plate. Although this method worked OK, results were not that consistent mainly because of issues related to confining the CdS vapor. Most of the time only the center the substrate got fully annealed due to the fact that the CdS vapor was not confined. In addition it was time consuming to prepare a fresh CdS source plate each time. To address these issues we developed a new scheme which gave very consistent results. This new scheme as shown in Fig 1 uses a CdS source boat instead of a source plate to generate the CdS vapor. Once filled the source material is good for annealing about 10 CTO films. This scheme was implemented in our RMS coater with very minimal modification to the carrier plate. We have already annealed over 40 CTO films using this new scheme. Light transmission and electrical properties of a typical CTO film annealed using this new scheme is shown in Fig. 2 and Table 1 respectively.

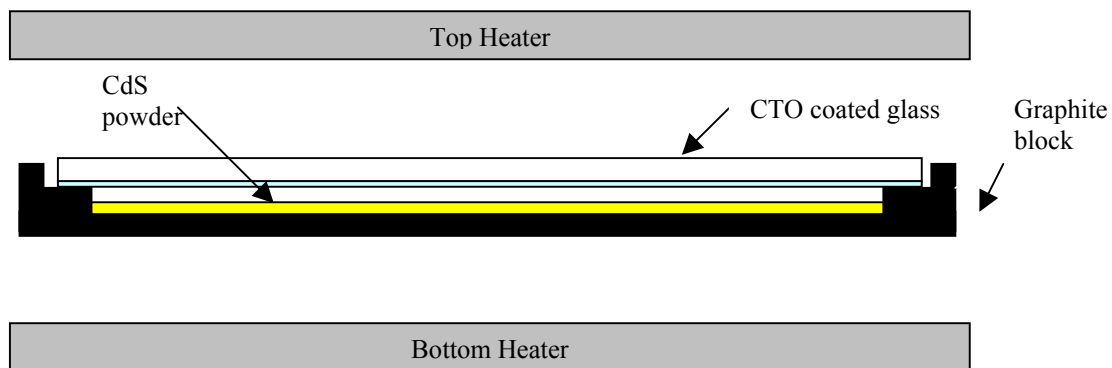


Fig. 1. CTO film annealing scheme

-Using higher pulse DC power (~300W) we were able to achieve growth rates as high as 500Å/minute. After annealing, the electro optical properties of these films were not any different from our standard films grown at about 200Å/minute.

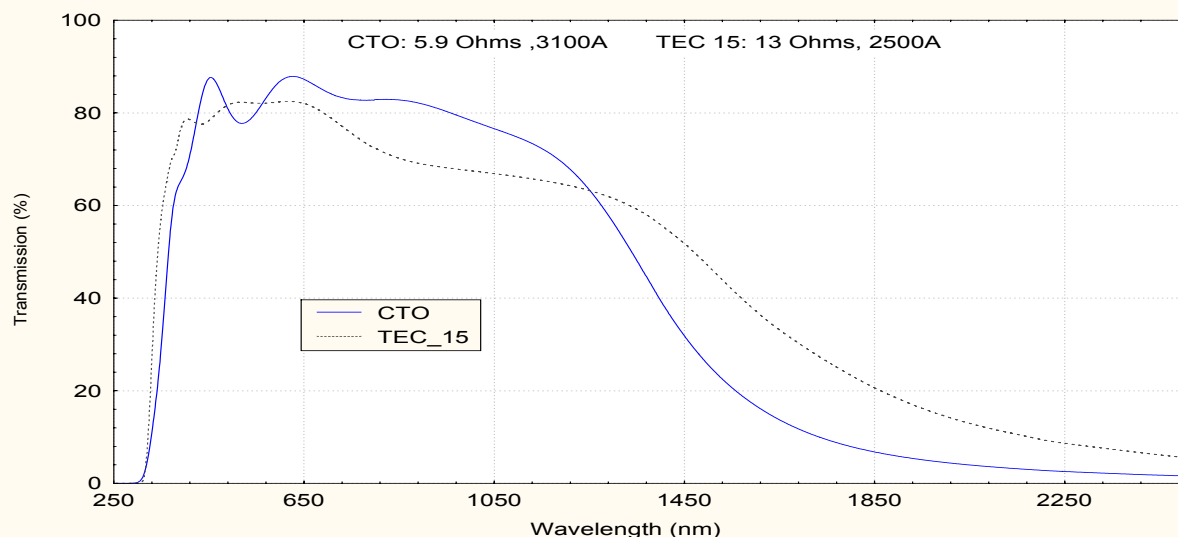


Fig 2 Transmission of TEC-15 glass and CTO-coated aluminosilicate glass of the same thickness.

	Thickness (Å)	n (cm-3)	Mobility (cm ² /V-s)	Res. (ohm-cm)	Sheet Resistance
CTO (FS)	3100	8.40E+20	40.4	1.85E-04	5.9
TEC-15	2500			4.50E-04	13

Table 1. Electrical properties of CTO compared to that of TEC 15 TCO

Zinc Stannate (ZTO)

- ZTO related work was slightly delayed due to a problem we had with the magnetron. The magnetron used to sputter ZTO was very early model (purchased in 1999) prototype version of the AJA ST 40 magnetron. As instructed by the manufacturer the magnetron head was replaced with a newer unit having max rate magnet configuration. With the new magnetron head the deposition rate was higher by almost a factor of three.
- As reported by Dr Wu [X. Wu, et al, 15th NCPV Photovoltaics Program Review, (AIP Conf. Proc. #462) p. 37], the as-deposited ZTO films were amorphous and very resistive (resistivity >5000 Ωcm). After annealing in a CdS environment at 570 °C for 1 minute (our standard deposition temperature and time) resistivity dropped to about 12 Ωcm. As grown or annealed ZTO films are very clear and have very little light absorption.

Sputtered a-CdS:O

- Sputtered a-CdS:O seems to give results comparable to our CSS CdS. For most of our work we have been using ~2% oxygen in the sputtering environment.

Cell Results

-The best cells made using the modified CTO/ZTO/a-CdS:O front contact structure had efficiencies ~14%. Cell parameters of few good cells are shown in Table 2. We are in the process of further optimizing the device structure in order to improve the cell efficiency beyond 14.5%.

Table 2

Cell (A025-2)	Eff (%)	Voc (mV)	Jsc (mA/cm ²)	FF (%)	Rsc (Ω -cm ²)	Roc (Ω -cm ²)
23	13.94	825	24.3	69.5	3438	5.1
34	13.84	816	24.9	68	143060	4.7

D. ZnTe:N, Cd_{1-x}Zn_xTe and Cd_{1-x}Mn_xTe Film Analysis

Brian E. McCandless and P. D. Paulson
for February 2003 to May 2003

Introduction

This report contains three sections, covering optical and structural properties of ZnTe:N, Cd_{1-x}Zn_xTe and Cd_{1-x}Mn_xTe thin films. Section 1 is a follow-up to the previous report (Dec02-Feb03) focusing on the properties of an annealed film UT62A. Section 2 contains results on Cd_{1-x}Zn_xTe and Cd_{1-x}Mn_xTe films deposited by sputtering at the University of Toledo. Section 3 contains results on Cd_{1-x}Zn_xTe films deposited by vapor transport at First Solar.

1. Annealed ZnTe:N film UT62A

Additional glancing incidence x-ray diffraction (GIXRD) measurements were made of film UT62A at incident beam angles (Ω) from 0.5, 1, 2 and 4° using Cu-K α radiation at 40kV and 40 mA (Figure 1). The film had been annealed in dry air at 350°C, which resulted in anomalous peaks in the diffraction pattern and were subsequently indexed as ZnO. Careful examination of the GIXRD data shows that the ZnO crystallographic orientation changes with incident beam angle. Sputtered ZnO films exhibit strong (002) texture in GIXRD measurements, as found for the scan of UT62A taken at 4°. Using this as an external standard, a thickness of 280Å was determined. Similarly, modeling the spectroscopic ellipsometry (SE) data for this film was only possible by inclusion of a 250Å thick ZnO layer with a roughness of 75Å. The GIXRD and SE data offer a consistent description of this sample.

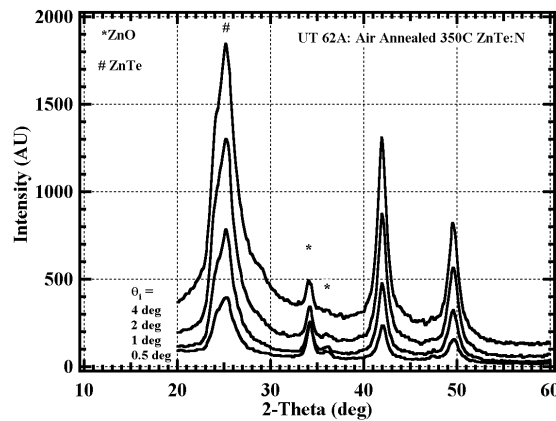


Figure 1. Glancing incidence diffraction patterns of UT62A at different incident beam angles.

2. $\text{Cd}_{1-x}\text{Zn}_x\text{Te}$ and $\text{Cd}_{1-x}\text{Mn}_x\text{Te}$ films deposited by sputtering at the University of Toledo

2.1 X-ray Diffraction

Symmetric and glancing incidence x-ray diffraction patterns were obtained for the two sputtered $\text{Cd}_{1-x}\text{Zn}_x\text{Te}$ films, CZT025 and CZT037 (Figure 2). In each case, reflections corresponding to the cubic form of the $\text{Cd}_{1-x}\text{Zn}_x\text{Te}$ alloy were found, with strong (111) texture. The satellite peaks on the low-angle side are instrumental. The position of the anomalous peak appearing at $\sim 49^\circ$ in the symmetric scans is consistent with the position of the other peaks and needs to be identified; one possibility is that it is a trace of hexagonal $\text{Cd}_{1-x}\text{Zn}_x\text{Te}$. No anomalous peaks were found on the surface. The position, intensities and FWHM of the (111) peak and corresponding lattice parameter and alloy composition are shown in Table 1 for the symmetric scans. The GIXRD scans show a single phase surface and a loss in crystallinity for the (220) and (311) reflections, which is explained by poor nucleation and low volume fraction of these orientations in the near-surface region for the incident angle used (0.5 deg).

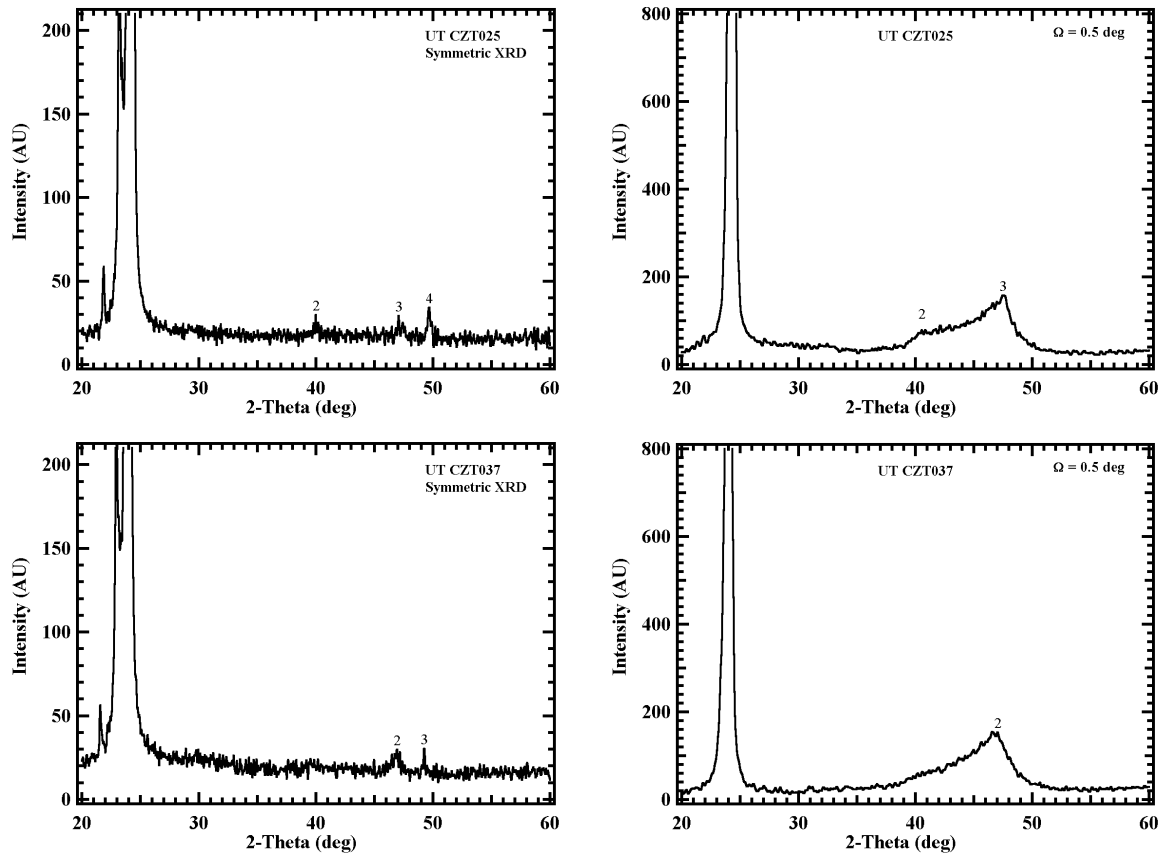


Figure 2. Symmetric x-ray diffraction (left) and glancing incidence x-ray diffraction (right) patterns of sputtered $\text{Cd}_{1-x}\text{Zn}_x\text{Te}$ films.

Table 1. $\text{Cd}_{1-x}\text{Zn}_x\text{Te}$ (111) position, intensity, FWHM, corresponding lattice parameter and alloy composition from symmetric XRD scans.

Sample	2θ ± 0.02 deg	I(111) (counts)	FWHM (111) (deg)	a_0 $\pm 0.005 \text{ \AA}$	x ± 0.05
CZT025	24.24	7300	0.17	6.35	0.30
CZT037	23.98	4800	0.20	6.42	0.20

Similar measurements were carried out for the $\text{Cd}_{1-x}\text{Mn}_x\text{Te}$ films (Figure 3). In this alloy system, there is a structural transition from zincblende to wurtzite at $x = 0.77$. Reduction of the cubic lattice parameter, obtained by Nelson-Riley-Sinclair-Taylor reduction of as many peaks as possible, was carried out using: $a_0 = 6.3590 \text{ \AA} + (1-x)(0.1355)$. The strong (111) texture and low FWHM are indicative of good crystallinity in these films.

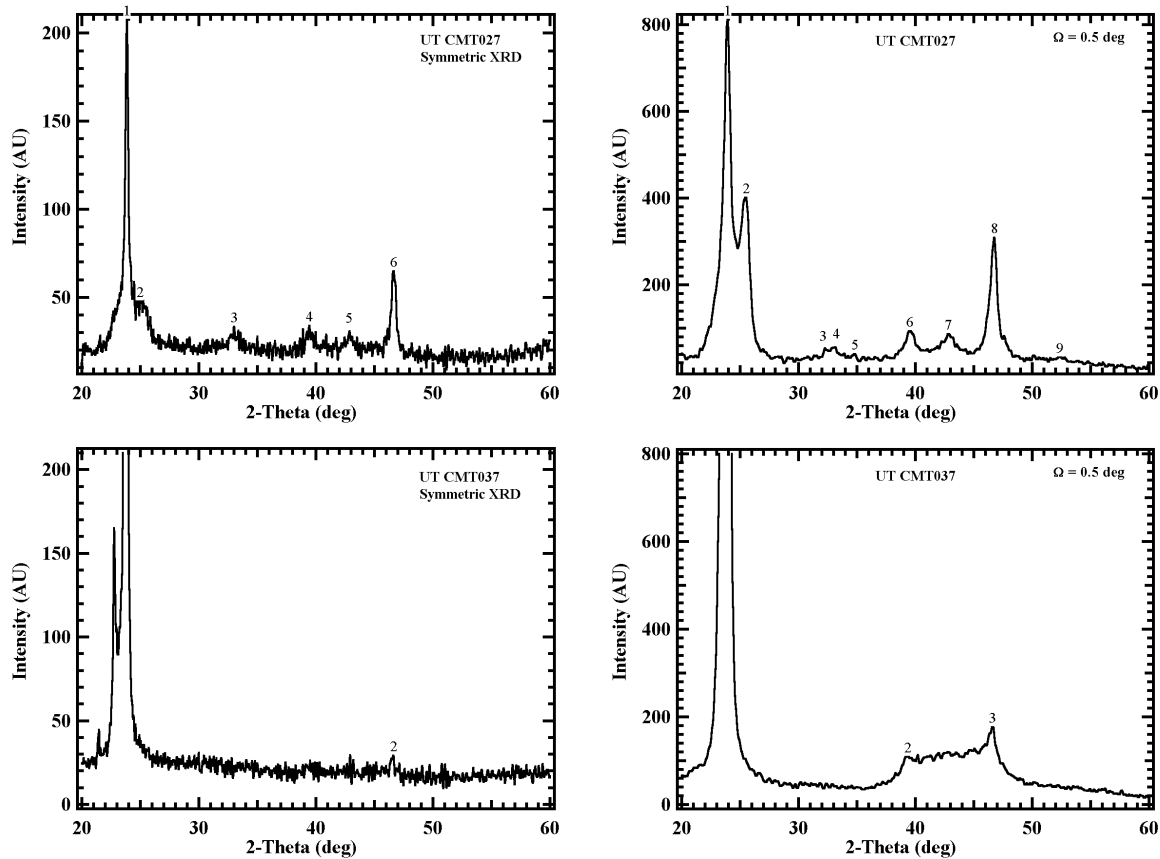


Figure 3. Symmetric x-ray diffraction (left) and glancing incidence x-ray diffraction (right) patterns of sputtered $\text{Cd}_{1-x}\text{Mn}_x\text{Te}$ films.

For film CMT027, the $\text{Cd}_{1-x}\text{Mn}_x\text{Te}$ (111), (220) and (311) peak intensities were low, and several secondary peaks were found in both symmetric and GIXRD scans. A preliminary analysis shows that the secondary peaks can be indexed as a distorted form of MnTe_2O_5 . This oxide appears to extend through the film. The low texture and large FWHM of film CMT027 indicate

poor crystallinity. Film CMT037, on the other hand, exhibits stronger (111) texture and a sharper line profile, indicating good crystallinity. The composition of the $\text{Cd}_{1-x}\text{Mn}_x\text{Te}$ films derived from the symmetric scans are listed in Table 2. GIXRD of CMT037 shows similar crystallinity trends for the (220) and (311) peaks at the surface, as found for the CZT films, although the peaks exhibit a *distribution* of coherency lengths and sharper edge profiles, suggesting better crystallinity than in the CZT films.

Table 2. $\text{Cd}_{1-x}\text{Mn}_x\text{Te}$ (111) position, intensity, FWHM, corresponding lattice parameter and alloy composition from symmetric XRD scans.

Sample	2θ ± 0.02 deg	I(111) (counts)	FWHM (111) (deg)	a_0 $\pm 0.005 \text{ \AA}$	x ± 0.05
CMT027	23.84	190	0.29	6.449	0.30
CMT037	23.78	3250	0.16	6.460	0.25

2.2 Spectroscopic Ellipsometry Analysis on $\text{Cd}_{1-x}\text{Zn}_x\text{Te}$ and $\text{Cd}_{1-x}\text{Mn}_x\text{Te}$ films

SE measurements were carried out between 0.73 eV to 4.6 eV using J. A. Woollam variable angle spectroscopic ellipsometer. Initial SE measurements show very poor dielectric responses on all but CZT037 films. The multilayer optical modeling results show the presence of a surface layer with thickness nearly 200 Å. All the films are highly specular and hence such a high surface layer thickness is unusual for this surface roughness. This is qualitatively consistent with the observation that the film surface is poorly crystallized and is therefore less polarized, manifested as a lower dielectric response. The possibility of an amorphous native oxide, such as found on CMT027 by GIXRD, cannot be ruled out also, and the chance of forming such an oxide on the surface could increase with the increasing amount of Zn and Mn in the alloy materials due to higher affinity of these cations with oxygen. In order to remove the surface oxides multiple short (~1 sec) rinses in weak $\text{Br}_2 + \text{CH}_3\text{OH}$ were carried out on these films. The rinse systematically improved the dielectric response, which was monitored by performing SE measurements after each rinse. No GIXRD measurements have yet been made after the rinse step. Figure 4a shows the effect of this rinse on the dielectric response of the film. As expected, the dielectric response of the films CMT027, CMT037 and CZT025 increased with increasing number of rinses. The dielectric response of CZT037 did not change significantly due to the etching indicates that the film is free of surface oxides. Interestingly the dielectric response of the CMT027 does not improve to the level of the remaining film and also by the end of second etching significant amount of Te formed on the surface.

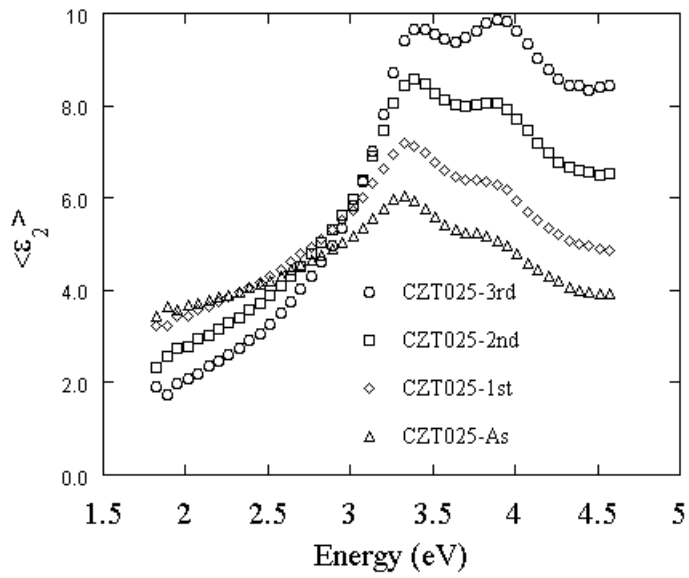


Figure 4a. Dielectric response of CZT025 before and after rinsing.

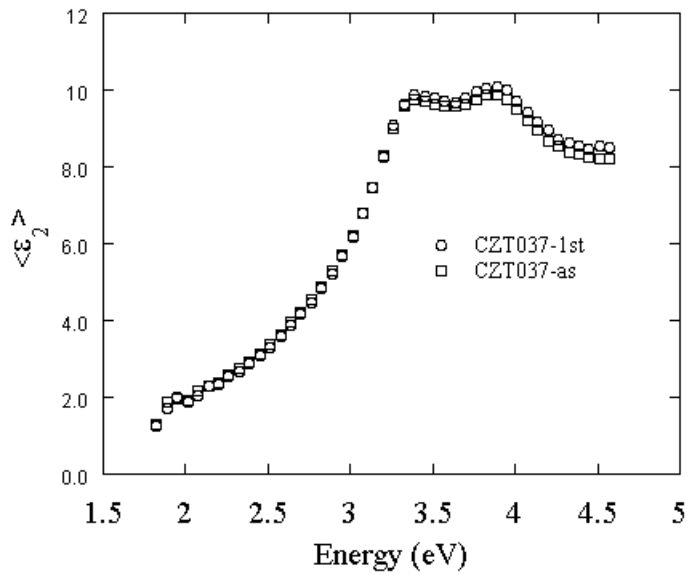


Figure 4b. Dielectric response of CZT037 before and after rinsing.

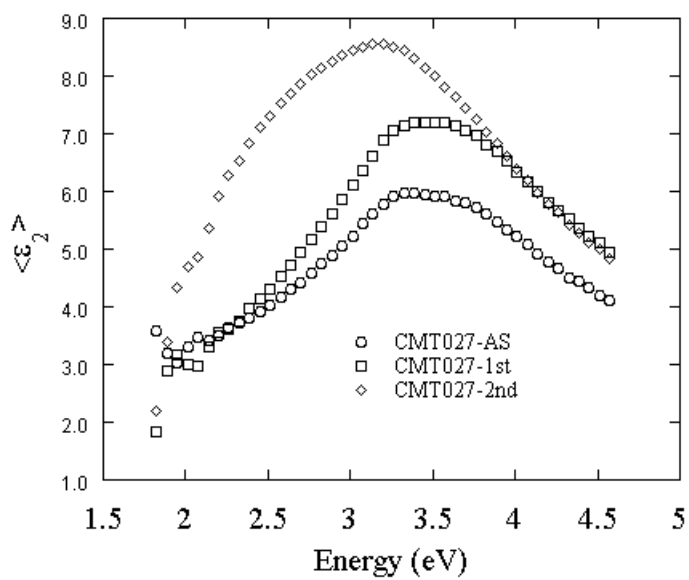


Figure 4c. Dielectric response of CMT027 before and after rinsing.

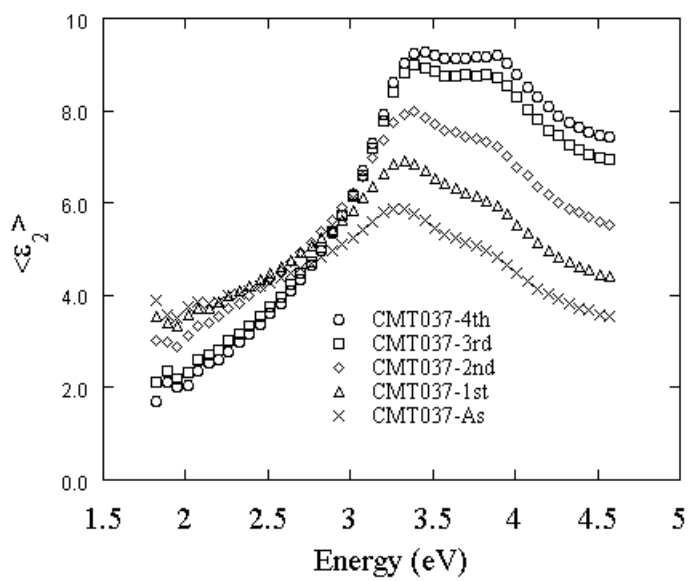


Figure 4d. Dielectric response of CMT037 before and after rinsing.

Optical modeling was performed on SE data showing the highest dielectric response, corresponds to least amount of the surface oxides on surface, for determining the optical constants. Figure 5 shows the optical constants of CZT037, CZT025, CMT037 and CMT027 films obtained from this analysis. Optical constants of CZT037 and CZT025 films are similar with critical points shift expected from the Zn/(Cd+Zn) ratio. However the index of refraction for CMT027 is slightly low compared to CMT037 indicating poor quality of film CMT027.

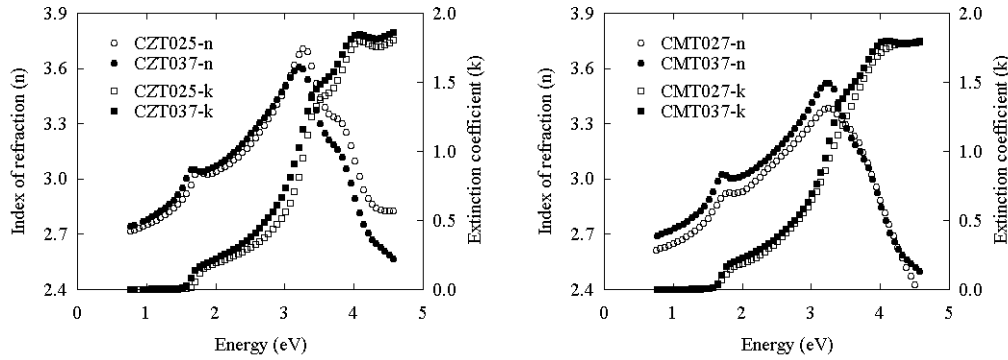


Figure 5. Optical constants for CZT and CMT films.

The energy corresponding to different electronic transitions are determined from the second derivative of the imaginary dielectric constants, which are shown in Figure 6. The critical points are shifted to higher energies consistent with the increasing amount of Zn and Mn in the films. Table 3 shows the energies of the various electronic transitions obtained from the different minima in the second derivative spectra. Critical point energies for CZT037 and CZT025 films shifted to higher energies with increasing Zn concentration. On the other hand for CMT027 film, E_1 and $E_1 + \Delta_1$ (eV) shows less energy compared to CMT037, which has more Mn. Also, the transition $E_0 + \Delta_0$ is not observed. These behavior could be the result of the presence of some other phases in the materials as shown by the XRD and GIXRD measurements.

In Table 3, the compositions of the CZT were determined from the transition energies using a semiconductor alloy model for the CdTe-ZnTe system [unpublished work]. For the CMT films, we do not propose compositions from the optical data, since no complete optical model yet exists.

Table 3. Electronic transitions and x for CZT037, CZT025, CMT037 and CMT027 films obtained from Figure 6.

Sample	E_0 (eV)	x ± 0.01	$E_0 + \Delta_0$ (eV)	E_1 (eV)	$E_1 + \Delta_1$ (eV)
CZT025	1.79	0.37	2.76	3.37	3.94
CZT037	1.71	0.22	2.66	3.34	3.91
CMT027	1.83	?	-	3.35	3.84
CMT037	1.76	?	2.63	3.36	3.92

3. $\text{Cd}_{1-x}\text{Zn}_x\text{Te}$ films deposited by vapor transport at First Solar, LLC

Similar characterizations were carried out on films FS03 and FS06 deposited by vapor transport (VTD) at First Solar, LLC. Preliminary results indicate the following:

- 1) Sample roughness precludes straightforward ellipsometry analysis, so spectrometric transmission and reflection were measured;
- 2) Both films exhibit band gap ~ 1.49 eV and lattice parameter $\sim 6.48\text{\AA}$, in both XRD and GIXRD measurements, suggesting very low incorporation of Zn in the zincblende lattice;
- 3) Sample FS03 exhibits a significant quantity of an undetermined secondary phase, with principal peaks at $2\text{-theta} = 31.75^\circ$ (2.816\AA), 34.35° (2.608\AA) and 36.1° (2.486\AA).

The optical transmission, reflection, normalized transmission, $T/(1-R)$, and absorption coefficient are shown below, compared to a PVD $\text{Cd}_{0.7}\text{Zn}_{0.3}\text{Te}$ film with similar thickness but specular surface morphology.

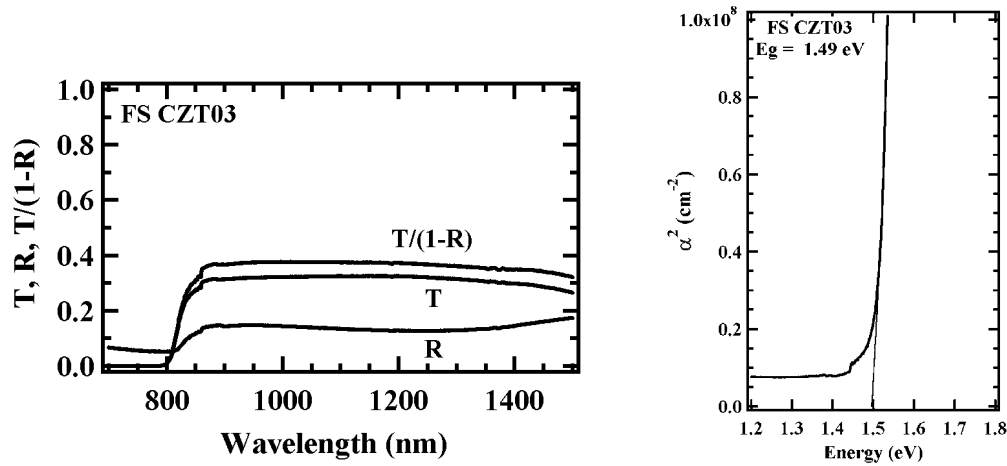


Figure 6. Optical properties of FS03 deposited by VTD.

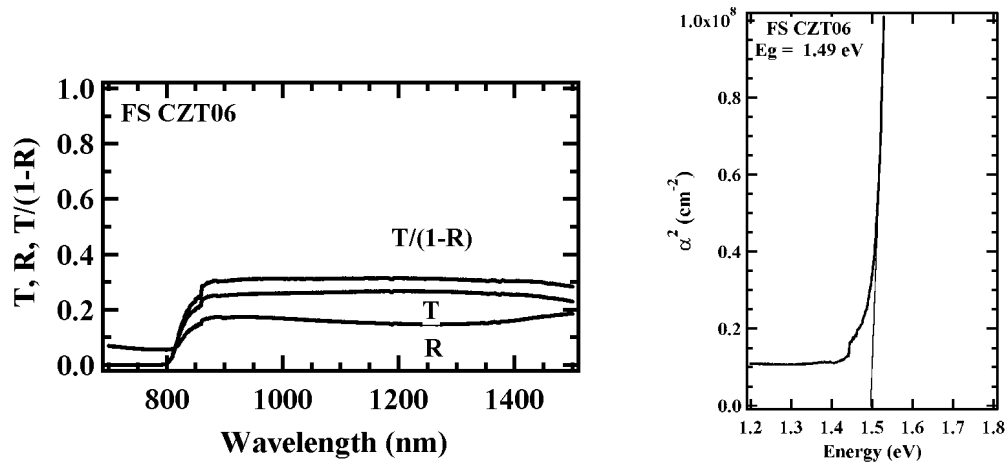


Figure 7. Optical properties of FS06 deposited by VTD.

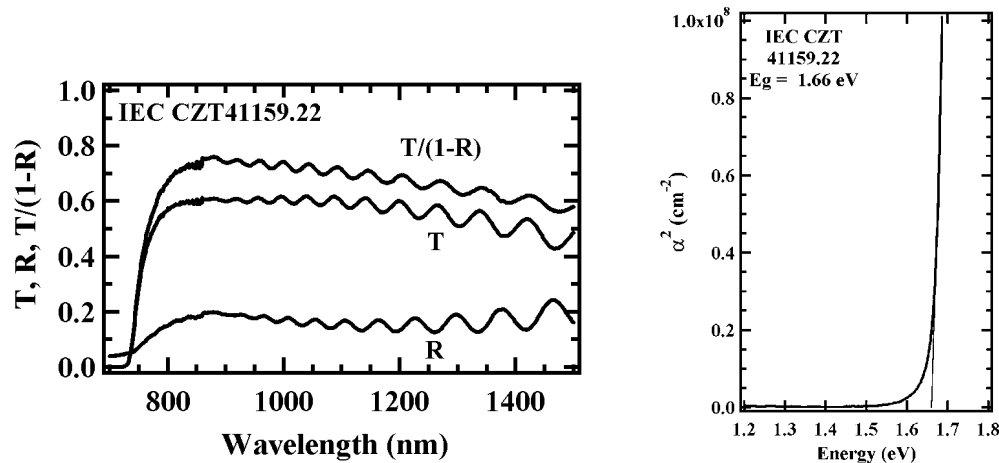


Figure 8. Optical properties of IEC41159.22, $x \sim 0.3$, deposited by VTD.

Sincerely,

Alvin D. Compaan, Principal Investigator

Copies to: Carolyn Lopez, Subcontract Associate, MS 2713, NREL
 Upali Jayamaha, Lower-tier subcontractor P.I.
 Brian McCandless, Lower-tier subcontractor P.I.
 Alvin Compaan, P.I., X. Deng, co-I
 Dorothy Spurlock, Director, Research and Sponsored Programs

Attachments: Preprint: A. Gupta and A.D. Compaan, "All sputtered 14% CdS/CdTe device with ZnO:Al front contact," oral paper 2O-C10-02, WCPEC-3

Preprint: A.D. Compaan, J. Drayton, V.Y. Parikh, G. Rich, A. Gupta, C. Taylor, Y. Yu, T. Osborn, and R.G. Bohn, "ZnTe:N/AnO:Al recombination junctions and stability properties of ZnTe:N and ZnO:Al," poster 2P-A8-31, WCPEC-3.